Steel and Composite Structures, *Vol. 22, No. 6 (2016) 1217-1238*
DOI: http://dx.doi.org/10.12989/scs.2016.22.6.1217

Studies on restoring force model of concrete filled steel tubular laced column to composite box-beam connections

Zhi Huang [1,2], Li-Zhong Jiang [*1], Wang-Bao Zhou [1b] and Shan Chen [3c]

[1] *School of Civil Engineering, Central South University, Changsha 410075, China*
[2] *Department of Civil Engineering, The Pennsylvania State University, Middletown 17057, PA, USA*
[3] *Hunan institute of nonferrous geological exploration and research, Changsha 410015, China*

(*Received April 15, 2016, Revised November 08, 2016, Accepted November 16, 2016*)

Abstract. Mega composite structure systems have been widely used in high rise buildings in China. Compared to other structures, this type of composite structure systems has a larger cross-section with less weight. Concrete filled steel tubular (CFST) laced column to box-beam connections are gaining popularity, in particular for the mega composite structure system in high rise buildings. To enable a better understanding of the destruction characteristics and aseismic performance of these connections, three different connection types of specimens including single-limb bracing, cross bracing and diaphragms for core area of connections were tested under low cyclic and reciprocating loading. Hysteresis curves and skeleton curves were obtained from cyclic loading tests under axial loading. Based on these tested curves, a new trilinear hysteretic restoring force model considering rigidity degradation is proposed for CFST laced column to box-beam connections in a mega composite structure system, including a trilinear skeleton model based on calculation, law of stiffness degradation and hysteresis rules. The trilinear hysteretic restoring force model is compared with the experimental results. The experimental data shows that the new hysteretic restoring force model tallies with the test curves well and can be referenced for elastic-plastic seismic analysis of CFST laced column to composite box-beam connection in a mega composite structure system.

Keywords: steel concrete composite connection; concrete filled steel tube (CFST); box-beam column connections; hysteretic restoring force model; seismic performance; connection behavior

1. Introduction

Mega composite structure systems are currently widely used in high rise buildings as lateral force resisting systems with their good structural performance, clear force transmitting, fast construction speed, eco-friendly and energy dissipation capacity of steel/concrete composite construction. This structure system could withstand the large cyclic forces generated during a severe earthquake. In addition, steel-concrete composite structures potentially increases the speed of construction and is eco-friendly material as it uses the recycled steel which has proven to be the promising material in the construction industry (Xue and Zhang 2014, Sabouri-Ghomi *et al*. 2016,

*Corresponding author, Professor, E-mail: lzhjiang@csu.edu.cn
[a] Ph.D., E-mail: huangzhi@csu.edu.cn
[b] Ph.D., E-mail: zhouwangbao@163.com
[c] P.E., E-mail: 459381985@qq.com

http://www.techno-press.org/?journal=scs&subpage=6 ISSN: 1229-9367 (Print), 1598-6233 (Online)

Denavit *et al*. 2016). Experimental and theoretical studies for the seismic performance of composite connections have been performed by researchers. Through previous available researches, experimental and analytical researches of CFST connections have been placed into two types: the most convenient connection by attaching the steel girder directly to the skin of the steel tube only (external connections) and other connections by attempting to transfer girder forces to the CFST column via embedded elements (internal connections). Yousef and Stephen (1996) has investigated the seismic performance of external connections based on experiments and numerical analysis. They found that the connections to the steel tube result in excessive distortion and could not meet the requirement of strength and stiffness characteristics during a severe earthquake. A significant amount of research has been done on the hysteretic performance of external CFT column to beam connections based on experiments and numerical analysis by Esfandyary *et al*. (2015). Stephen and Yousef (1998) extended the connections using embedded elements to distribute the girder flange force to the concrete core and performed experiments on behavior of connections to CFSTs. The results of experiments exhibited good cyclic performance with favorable inelastic characters. And then, Jason *et al*. presented the details of experimental results of the internal connections to investigate the behavior of composite column-to-beam connections using four specimens under monotonic loading (Jason *et al*. 2001) and six specimens under cyclic loading (Jason *et al*. 2002). They found that the strength and stiffness of internal connections was adequate to meet the seismic requirement as a rigid connection. In addition, Kataoka and El Debs (2015) improved the beam-column internal connections by embedding bolts and developed the accompanying design provisions. They presented the experimental results for three large-scale connection specimens and proposed a new design model for the internal connections. After extensive cyclic loading experiments, Wu *et al*. (2015) proposed a full bolted diaphragm-through connection which could be applied to H shape steel beam to CFST columns with their good seismic behaviors and also presented the quasi-static experimental results of four full-scale connection specimens of the new connection. Kang *et al*. (2015) compared joint shear strength with internal diaphragm connections to CCFT columns by use of ABAQUS and OpenSEEs and proposed a modified joint shear force-deformation relations. In order to verify the destruction characteristics and aseismic performance of joints composed of CFST lattice columns and composite box girders in mega-composite structure system, Jiang *et al*. (2014) presented the experimental results of three different connection types including single limb bracing, cross bracing and diaphragms at the core area of joints.

When it comes to the restoring force model of CFST laced column to composite box-beam connections. Current design practices for these connections heavily rely on the judgement and experience of individual designers, as little research information is available. The available literature researches on connection characteristic parameter are based on the experimental studies for ordinary reinforced concrete structures and/or steel-concrete composite column to steel beam connection. For examples, Men *et al*. (2015) analyzed the seismic performance of novel composite frame connections based on the six composite reinforced concrete column-to-steel beam interior joints experiment researches. Li and Cui (2008) carried out a low cyclic pseudo-static test for four one-fourth scale specimens of shear wall supported on the steel reinforced frame and proposed the three trilinear restoring models under monotonic loading and cyclic loading taking into account the degradation of strength and stiffness. And then, Xu and Nie (2011) presented the experimental study of connections of concrete-filled square steel tubular columns with continuous diaphragms and investigated the seismic behavior of this connection. The test results showed that the connections with continuous diaphragms failed in ductile mode and had the sufficient energy

dissipation capacity and ductility.

The CFST connections can be divided into five basic types: ring strengthening connections, anchoring connections, through-tube corbel connections, through-diaphragm connections and rebar-enclosed connections. In recent years, the connections with ring stiffeners described in this paper is widely used in the concrete-filled steel tube structure of the high-rise and super high-rise buildings, like Taipei 101 in Taipei, Shanghai World Financial Center, and Shanghai Tower in China. Its mechanism can be simply explained as that the upper and lower ring plates are installed respectively to the upper and lower flanges of the beam located on the top of the Concrete-filled steel tubular column. And then the upper and lower ring plates are welded or are tightened by high strength bolts to the upper and lower flanges of the steel beam respectively in order that the bending moment at the end of the beam is transited to columns. And also a vertical steel rib slab is welded to the position between the upper and lower ring plates so that the shear force of the end of beam can be transited. In earthquake areas, the structural design should meet the principle of "strong-joint weak-member", so that the beam-column connections can undergo large plastic deformation during a severe earthquake, and the earthquake energy can be absorbed by the plastic deformation. If the bearing capacity of the connection is larger than the yield load of the beam and column, the plastic region can be extended along the length of the beam and column, which would play an important role in the energy dissipation and ductility of the structure. Otherwise, the damage will be occurred at the connection area. Furthermore, the connection with ring stiffeners is also one of the recommended joint types for the design and construction of CFST structures by Chinese specification CECS28: 2012. And the construction details of the connections are an important issue for structural design, especially for the mechanism properties and stability of the whole mega composite structure system. Therefore, this paper focused on three new different connection types with different construction details, and discussed their seismic performance.

As a part of the research project "High rise mega composite structure under cyclic dynamic and severe earthquake actions", the main objective of this research is to develop a procedure to improve the analysis method of a composite column to beam connections in mega composite structural buildings and obtain the hysteretic performance. In order to provide a theoretical reference for this new structural elastic-plastic time-history analysis, based on the pseudo-static test research, combined with theoretical analysis of hysteretic curve and restoring force characteristics for CFST laced column to composite box-beam connections, this study aims to obtain a new hysteretic restoring force model.

2. Experiment procedure

2.1 Specimen preparation

Composite connections are typically designed for the high rise buildings in earthquake-prone areas. Therefore, this research is interested in three different connection types of side column including single limb bracing, cross bracing and diaphragms in the core area of connections. The prototype specimens were tested under low cyclic and reciprocating loading.

Fig. 1 shows the connection details. Each composite box-beam was fabricated using a 6mm thickness steel plate with the yield strength of 235 MPa (Q235B). The total height of the beam = 270 mm including 80 mm thickness concrete flange plates. The flanges of the beam were directly connected to the box-girder via complete-sheer bolts with grade-4.6 13 mm Φ bars and arranged

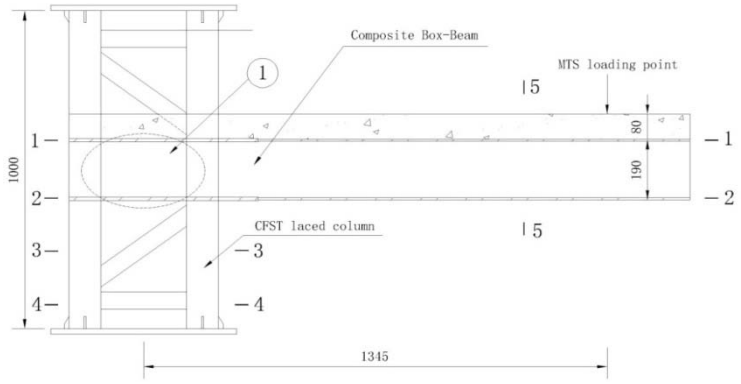

(a) Elevation of connections

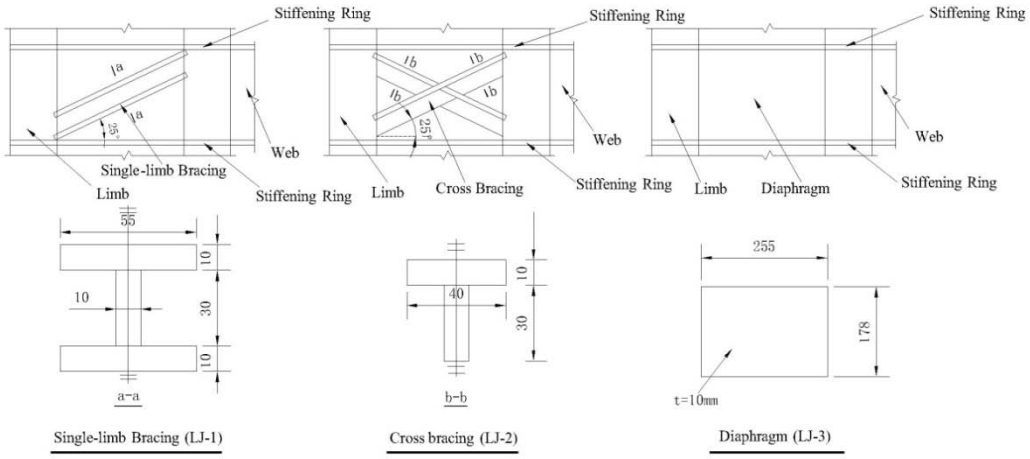

(b) Connection types of specimens

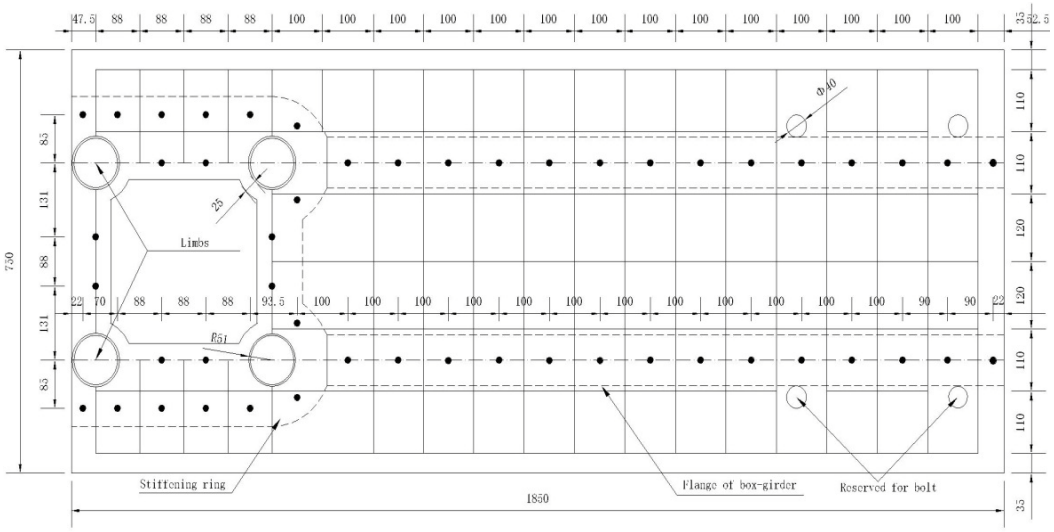

(c) Sectional drawing 1-1 (Concrete, Reinforcements, and Upper flange of box-girder)

Fig. 1 Geometry of test specimens (*Notes: All units in mm)

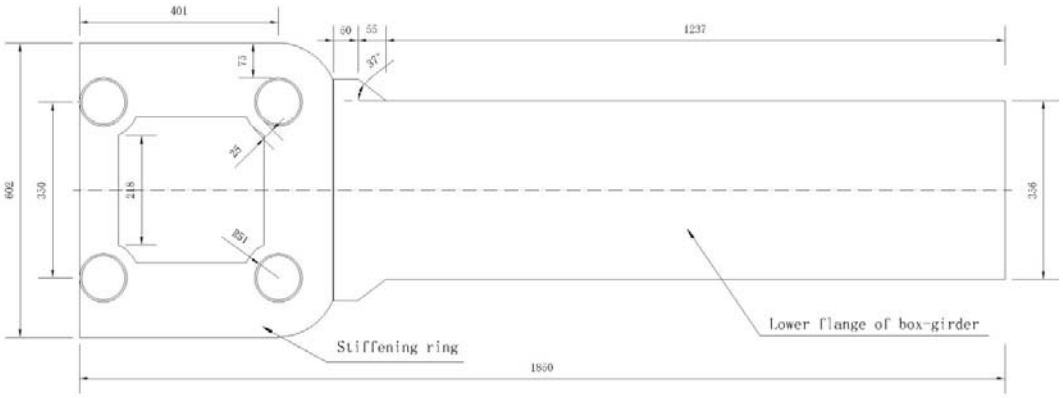

(d) Sectional drawing 2-2 (Lower flange of box-girder)

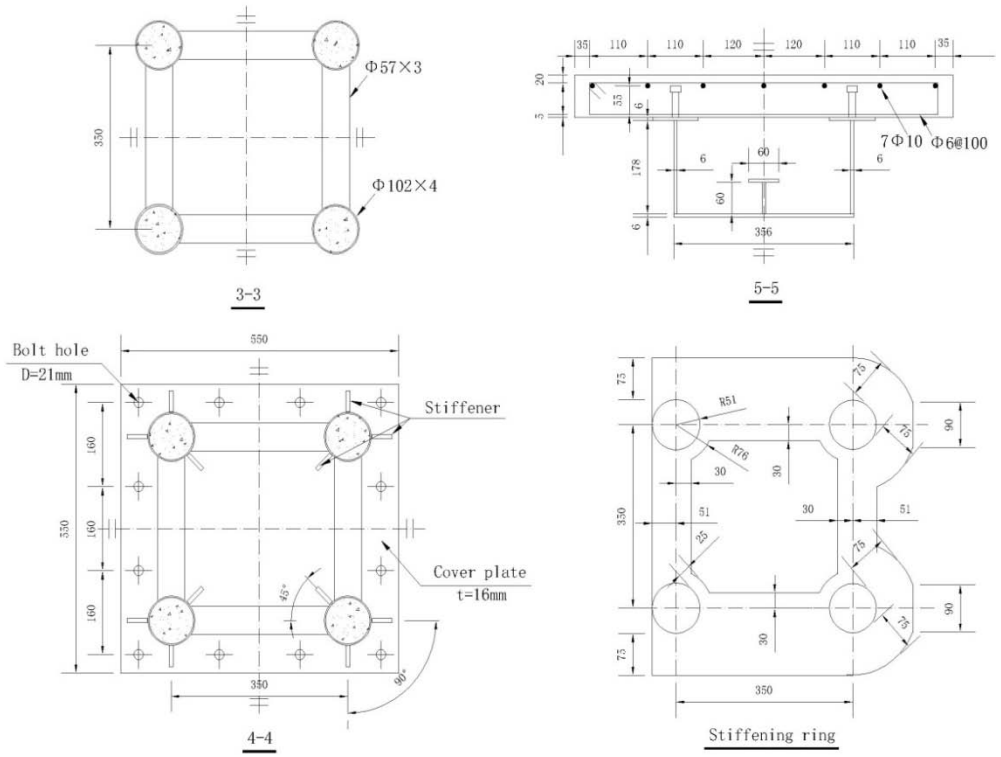

(e) Sectional drawing 3-3, 4-4, 5-5 and size of stiffening ring

Fig. 1 Continued

one sheer bolt per 100 mm as indicated in detail in Table 1. The concrete compressive strength of all specimens = 30 MPa, which is widely used in composite structure. And the concrete flanges were cast with adequately reinforced concrete using 10 mm B longitudinal bars (HRB335) and 6 mm A stirrups (HPB235). The total height of CFST laced column = 1000 mm, and the arm-length between the center of columns and the loading point at the end of the beam = 1375 mm, as shown in Fig. 1. The steel limbs were cut from a seamless steel tube with the grade-20# and filled with

Table 1 Specimen descriptions

Specimen	LJ-1	LJ-2	LJ-3
Connections in core area	Single-limb bracing	Cross bracing	Diaphragm
Limbs ($D \times t$)		Ø102 × 4	
Tubes ($d \times t'$)		Ø57 × 3	
Angle between tubes		53°	
Box-girder ($h \times b \times t_w \times t_f$)		190 × 350 × 6 × 6	
Concrete flange ($b_c \times h_c$)		750 × 80	
Longitudinal bars		B 10@110	
Stirrups		A 6@100	
Studs		A 13@100	
Thickness (t)		10	
Width of stiffening ring (b)		75	
Axial pressure (kN)		730	
Axial compression ratio (n)		0.3	

*Notes: All units in mm; A and B = bar diameters represent stirrups of HPB 235 plain steel bar and HRB 335 hot rolling ribbed reinforcing bar, respectively

self-compacting concrete with the compressive strength 30 MPa. All steel-strength plates and node connectors used were weld of grade 345 MPa yield strength with 10mm thickness.

The steel part of the specimens were welded of steel pipe latticed column, composite box-girder and stiffening ring using double-sided arc welding (DSAW). All of the studs of box-girder were welded to the face of flange plate in a single row along the longitudinal direction of the beam as shown in Fig. 1(c). And the stiffeners were arranged in the foot of the CFST laced columns shown as Fig. 1(e) to ensure that the local buckling strength of the specimen could be achieved.

According to China's test specifications and standards (GB/T 50081 2002), the design concrete compressive strength f_{cu} of 150 mm × 150 mm × 150 mm cubic samples and the concrete elastic modulus E_c of 100 mm × 100 mm × 300 mm samples must be obtained. Through the measured f_{cu} values, we can obtain the axial compressive strength f_c of concrete using the empirical formula, Eq. (1) (Guo 1998). The average mechanical properties of concrete are listed in Table 2, in which the specimens were cast at the same time and maintained under the same condition.

$$f_c = 0.76 f_{cu} \tag{1}$$

The average yield strength f_y and ultimate strength f_u of reinforcing steel are presented in Table 3, which were obtained from tensile strength tests according to the test specifications and standards (GB/T2975 1998) in China. The yield strength of studs was obtained from the tests according to the test specification (GB/T10433 2002).

Table 2 Average compressive strength of concrete

Core concrete in limbs			Concrete in box-girder flanges		
f_{cu} (Mpa)	f_c (Mpa)	E_c (Mpa)	f_{cu} (Mpa)	f_c (Mpa)	E_c (Mpa)
31.2	23.7	23800	35.5	27.0	31470

Table 3 Average mechanical properties of reinforcing steel

Steel	Thickness/diameter (mm)	Measured dimension (mm)	Yield strength f_y (N/mm^2)	Ultimate strength f_u (N/mm^2)
Limbs Ø102	4.0	4.20	305	431
Tubes Ø57	3.0	3.22	258	422.5
Plate (Q345)	10.0	9.40	455	537.5
Plate (Q235)	6.0	5.66	324	465
Longitudinal bars	10.0	9.24	547	637
Stirrups	6	5.12	428	529

* Notes: Q345 and Q235 represent grade of steel plate

2.2 Test setup and loading history

Each connection specimen was loaded with a reaction frame and tested in the vertical plane as depicted in the Fig. 2. For the CFST laced column, both the top and bottom connections used blade hinge to keep the column ends rotate freely. A jack was placed at the top of the column to produce the initial 2000 kN constant vertical axial loading. For the box-beam, a special loading plate was placed at the loading point both on the upper and lower surface of the box-beam at the end of the beam. And the loading plate was anchored with MTS actuator. The MTS system includes a 1000 kN vertical servo actuator to generate the vertical loading with ±30 mm stroke shown in Fig. 2. The data acquisition records displacements, loads and strains, inputs from the strain gauges on box-girder, longitudinal bars, stirrups, and node connectors and detects possible displacements and rotations at the base. Strain gauges were also adhered to the surface of the column, box-beam and along with the bars in a number of predetermined before the specimens were built.

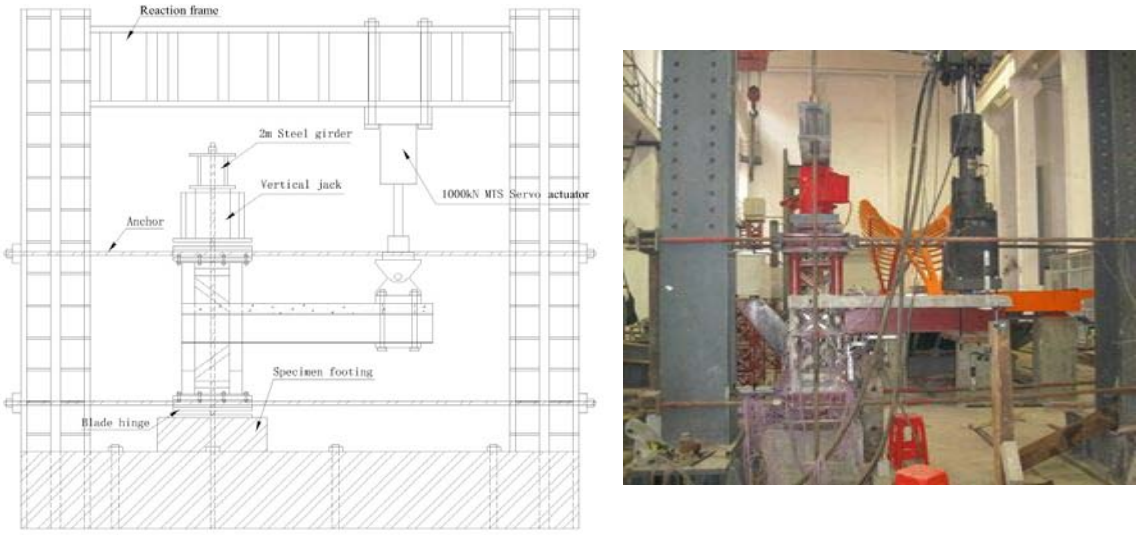

(a) Schematic layout (b) Overview

Fig. 2 Test setup

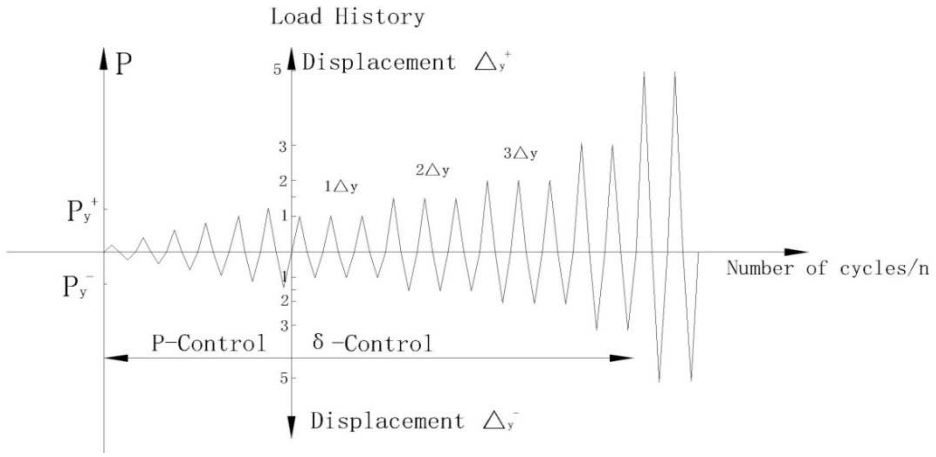

Fig. 3 Cyclic load history

Before the cyclic loading, the CFST laced column was preloaded twice to 20% of the intended test axial load to confirm the proper function of the equipment and gauges. Meanwhile, this process assured that all apparatus and instruments were working and reliable. After the alignment, the load was kept constant to the axial compressive force of CFST laced columns and the test started. Pressure was continued applied for 2-3 minutes.

Pseudo-static loading mode has been carried out for this test. Fig. 3 shows the typical history that consists of two stepwise stages. The first stage applied to the specimen, vertical loading at the end of the box-beam applied in equal incremental ΔF (Force) every cycle until specimen yield, were elastic and were regulated under load control. JGJ101-96 (1996) and ATC-24 (1992) suggest that force rather than deflection control is used for the first stage as the specimen may have very high initial stiffness at the elastic stage, and deformations may be difficult to predict and control. The cycles at the second stage were then followed by inelastic cycles, which were regulated under deflection control. The amplitude for each step increased by the yield displacement of the specimen e.g., $1\Delta y$, $2\Delta y$, $3\Delta y$, $4\Delta y$, ……. Three cycles were completed for each step until terminated.

As the mechanical properties of composite box-beam forward section is not the same as the reverse one when applying cyclic loading, so that the composite box-beam display a different positive and negative yield load and displacement during the experiments. Considering that, the forward cyclic load refers to the positive yield load Δ_y^+ and yield displacement P_y^+ (where the compression of concrete is positive); however, the reverse cyclic load refers to the reverse ones, Δ_y^- and P_y^- respectively. After determining the ultimate load $P_{\max}$ defined as the maximum strength calculated by using nonlinear finite element theory, the yield displacement Δy can be defined as the displacement point corresponding to the force of $0.7P_{\max}$. And the displacement Δy applied to the specimens should be timely adjusted according to the test result during the experiment.

When it approaches the critical state of a specimen failure, the load will go down as well as significantly increased displacement phenomenon. If any of the following situation occurs, the specimen is considered as a failure and the loading should be terminated (Wang 2006).

(a) The composite box-beam or the CFST laced column failures.
(b) A visible drum deformation is detected at the connection core area.

(c) Lateral torsional buckling is detected at the column and/or box-beam.
(d) Failure phenomenon is indicated at the connection area e.g., steel yield, tearing and/or local failure of welding.
(e) Load decrease to the 85% of the peak value.

2.3 Experimental results and hysteretic curves

The results of the cyclic tests are presented in this section, especially for the hysteretic curves. Specimens LJ-1, LJ-2 and LJ-3 underwent a very similar destruction process to its cyclic counterpart. It shows the weak-beam failure mechanism, which means the destruction of the connections formed and propagated from the welded place connected the upper flange of the steel box-girder and stiffening ring. A transverse crack started at -20kN (see Fig. 4), and many transverse cracks developed by Δ_y^- along the entire length from the beam flange to MTS load point (see Fig. 5). Then, the specimen turned into plastic stage, loading by displacement control. When the displacement reaches $3.0\Delta_y^+ \sim 4.0\Delta_y^+$, an inclined longitudinal crack was observed in the surface of concrete plate at the bottom of the column. At this time, there is a weld crack observed as the cross bracing at the connection core area bearing too much tensile stress for specimen LJ-2. Reverse increasing the displacement to $4\Delta_y^-$, fracture starts from the weld between the steel girder and stiffening ring and tearing appears on the surface of the web. There is an obvious decrease for

Fig. 4 The first crack in the concrete flange

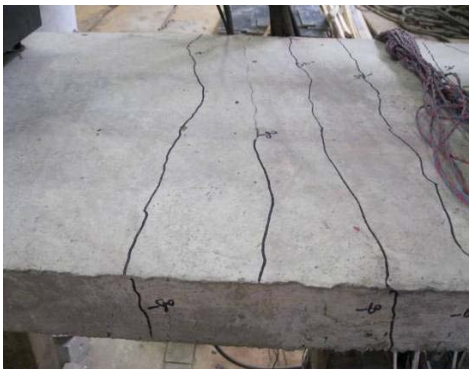

Fig. 5 Cracks developing of the concrete flange

Fig. 6 Weld fracture at the box-girder flange

Fig. 7 Concrete flange transverse fracture

Fig. 8 Torn-crack in the web of box-girder

Fig. 9 Typical failure mode of specimens

reverse bearing capacity along with the weld fracture, result in the concrete flange broken at the stiffening ring, indicating the connection starts failure (see Fig. 6 and 7). Increasing the displacement to $5.0\Delta_y^+$, the broken concrete plate bearing the compressive stress again, and the tearing steel web appears drum deformation due to the compressive stress, along with decreasing positive bearing capacity. Reverse increasing the displacement to $5.0\Delta_y^-$, the concrete plate has been crushed, torn cracks in the web of box-girder bigger and bigger (see Fig. 8). At this point, the loading is terminated due to connection specimen failure as shown in Fig. 9. The experimental results show that the steel stiffening ring, joint connectors and CFST laced columns of specimens work well, indicating that the design of connections sufficiently meet the objective of "strong-column weak-beam".

In this study, load versus box-beam tip displacement ($P-\Delta$) response has been used to compare the performance of each connection. The relationship between load and beam tip deflection is defined as hysteretic curve, it usually takes into account the capacity of dissipated energy and is usually qualitatively analyzed in the seismic performance of a structural member or system. In these plots, load (P) is obtained by the sensor installed inside the MTS actuator at the loading point of the beam. The box-beam tip displacement (Δ) measured with displacement meters at the loading point.

Fig. 10 shows the box-beam tip response for specimens LJ-1, LJ-2 and LJ-3, respectively. During the elastic range, the deformation is nearly 100 percent recovered and no residual deformation after unloading, and the area enclosed by the hysteretic loops, which represent energy dissipation, could be negligible. The change of the integral rigidity is tiny, substantially considering as a linear loop. As the loading increase, the curve came into nonlinear with a declining slop gradient, indicating the specimens connection come into plastic deformation. The stiffness started decrease and the shape of curves gradually became gentle slope. However, the displacement increased rapidly and residual deformation appeared after unloading. When the specimens came to yield, the beam tip load decreased with the cyclic loading and the slope of the hysteretic curve gradually reduced indicating the stiffness kept degrading. At the same time, the strength of the specimen connection began degrade too. The resultant failure mechanism for each specimen was identical, but the underlying reasons for its formation were different. As the displacement increased, the capacity of specimen's energy dissipation decreased gradually with an obvious pinch phenomenon because of the drum deformation in the web and opening-closing of cracks of concrete during the cyclic loading test.

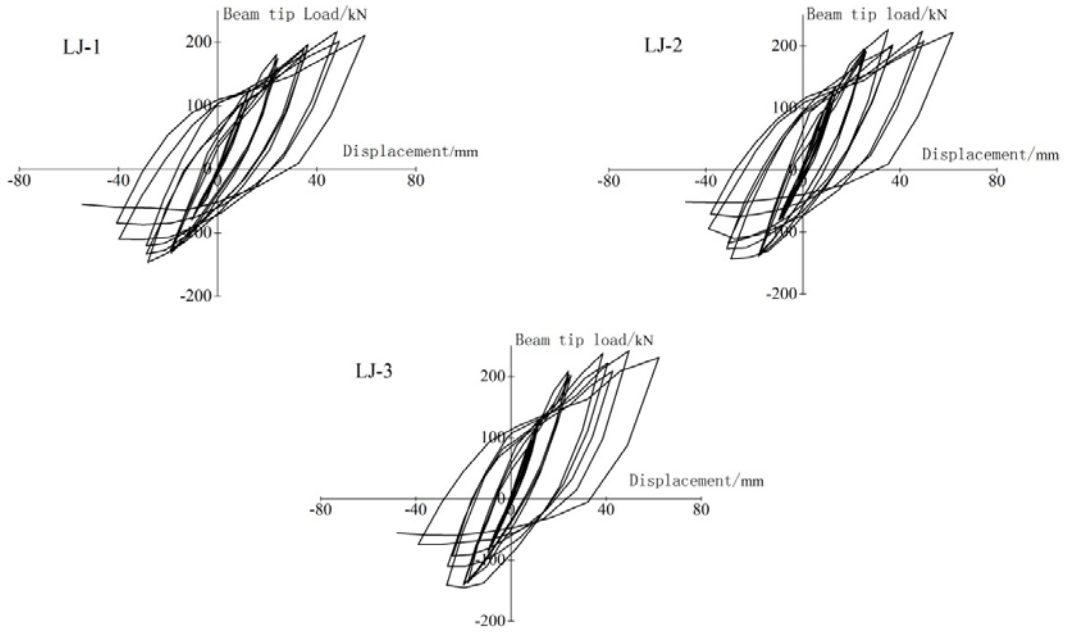

Fig. 10 Load versus beam tip displacement (*P*-Δ) hysteretic curves of the specimens

2.4 Skeleton curve

A skeleton curve is commonly defined as the envelope of the force-displacement curve, i.e., the path of the successive peaks of the first cycle at each load level (Zhang *et al*. 2012). It is usually used to characterize the hysteretic behavior and ductility capacity of steel and/or steel-concrete composite members subjected to load reversals. The skeleton curves of the test specimens are shown in Fig. 11.

As seen, the skeleton curves consist of three stages: initial elastic, elastic-plastic, and plastic with decreased stage. The positive downtrend rates of skeleton curves of the specimens are slower than the negative downtrend, indicating that the plastic behavior is better than the negative one.

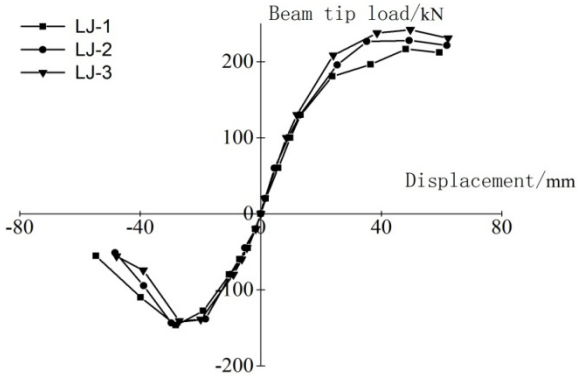

Fig. 11 Load versus beam tip displacement skeleton curves of the specimens

The stronger the construction of the connection style is, the larger the stiffness during the elastic stage, and so did the positive bearing capacity and ultimate bearing capacity, as evidenced from the lower yield displacement while positive loading. This is because the core area of specimen LJ-3 tends to be solid connection under the condition of the strengthening of the connection construction, and the solid connection has a greater rigidity compared with other lattice connection (Specimens LJ-1 and LJ-2). However, when reverse loading, the strength and failure displacement of connection specimens decrease gradually but it is not obvious. The above results caused by the different tensile-compression performances of the concrete flange plate of the steel-concrete composite box-girder.

3. Numerical analysis and discussion

3.1 Constitutive model of materials

The accuracy of simulation of connections' behavior is strongly determined by the concrete constitutive model used, particularly in terms of the nonlinear behavior, as well as the convergence of numerical analysis. In the plastic damage's study of concrete within ABAQUS, the three widely adopted concrete constitutive models, including smeared cracking model, damaged plasticity model and cracking model of concrete, are used to predict the elastic-plastic and nonlinear behavior of concrete columns under low cyclic loading. The concrete constitutive model in the core area is adopted here with reference to the damaged plasticity model (Yu and Ding 2003). The monotonic concrete stress-strain relation under the compression loading is described as the following Eq. (2) (Liu 2005).

$$y=\begin{cases}2x-x^2 & x\le 1\\ \dfrac{x}{\beta_0(x-1)^2+x} & x>1\end{cases} \tag{2}$$

With $x=\dfrac{\varepsilon}{\varepsilon_0}$, $y=\dfrac{\sigma}{\sigma_0}$, $\sigma_0=f_c$, $\xi=\dfrac{A_s f_y}{A_c f_{ck}}$, $\varepsilon_c=(1300+12.5\times f_c)\times 10^{-6}$, $\varepsilon_0=\varepsilon_c+800\times\xi^{0.2}\times 10^{-6}$, $\beta_0=(2.36\times 10^{-5})^{\left[0.25+(\xi-0.5)^{7.0}\right]}\times f_c^{0.5}\times 0.5\ge 0.12$

Where f_c is the compressive strength of concrete cylinder of $\emptyset 150\times 300$ mm, ξ is the confinement factor of concrete in the core area.

The monotonic concrete stress-strain relation under the tension loading is described as below Eq. (3), used for skeleton curves in the concrete core tension area.

$$y=\begin{cases}1.2x-0.2x^6 & x\le 1\\ \dfrac{x}{0.31\sigma_p^2(x-1)^{1.7}+x} & x>1\end{cases} \tag{3}$$

With $x=\dfrac{\varepsilon}{\varepsilon_p}$, $y=\dfrac{\sigma}{\sigma_p}$

Where $\sigma_p=0.26\times(1.25 f_c)^{2/3}$, $\varepsilon_p=43.1\times\sigma_p\times 10^{-6}$, $E_c=4730\sqrt{f_c}$.

Compared to the concrete model, the steel models are different from the loading mode and it

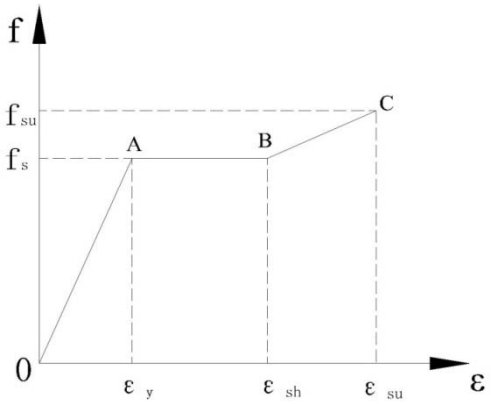

Fig. 12 Stress and strain relationship of steel

includes trilinear model, isotropic hardening model, kinematic hardening model and mixed hardening model. In this study, the constitutive model is adopted here with reference to the simply trilinear model. The following Eq. (4) describes the stress-strain relationship.

$$\sigma = \begin{cases} E_s \varepsilon & 0 < \varepsilon \le \varepsilon_y \\ f_s & \varepsilon_y < \varepsilon \le \varepsilon_{sh} \\ f_s + (\varepsilon - \varepsilon_{sh}) E_{st} & \varepsilon > \varepsilon_{sh} \end{cases} \tag{4}$$

Where E_s represents the elastic modulus of the steel, $E_{st} = 0.01E_s$ is the elastic modulus after the steel strengthened. The relationship of the parameters ε_{sh}, f_s, ε_y are shown in Fig. 12.

3.2 Comparison between numerical and experimental results

To verify the finite element model used for numerical simulation, the hysteretic curves of the force-displacement relationship of the specimens analyzed with the constitutive models of materials were compared with the experimental results in Fig. 13. The experimental results are indicated by a solid line, while the numerical values are displayed by a dashed line.

The comparison shows that the cyclic behaviors of the connections are fairly well. Overall, the hysteresis curves appear in a spindle shape (see Fig. 13), and the hysteresis loops are plump and just slight pinching phenomenon, indicating that the plastic deformation capacity and energy dissipation capacity of this kind of connections are good. They are showing a good seismic performance.

According to the test and numerical analysis results, the failure processes of three kinds of connections are similar: the failure occurs at the end of the box-beam where the upper flange plate of box-beam welded to the strengthening ring. At the same time, the steel stiffening ring, joint connectors and CFST laced columns of specimens all show a good performance, which is weak-beam failure mechanism, and meets the design objective of “strong-column weak-beam”.

The numerical model is in good agreement with the experimental results, which shows that the constitutive model and the modeling method can simulate this kind of connections well, and can be used for the further analysis of the parameters of the connections.

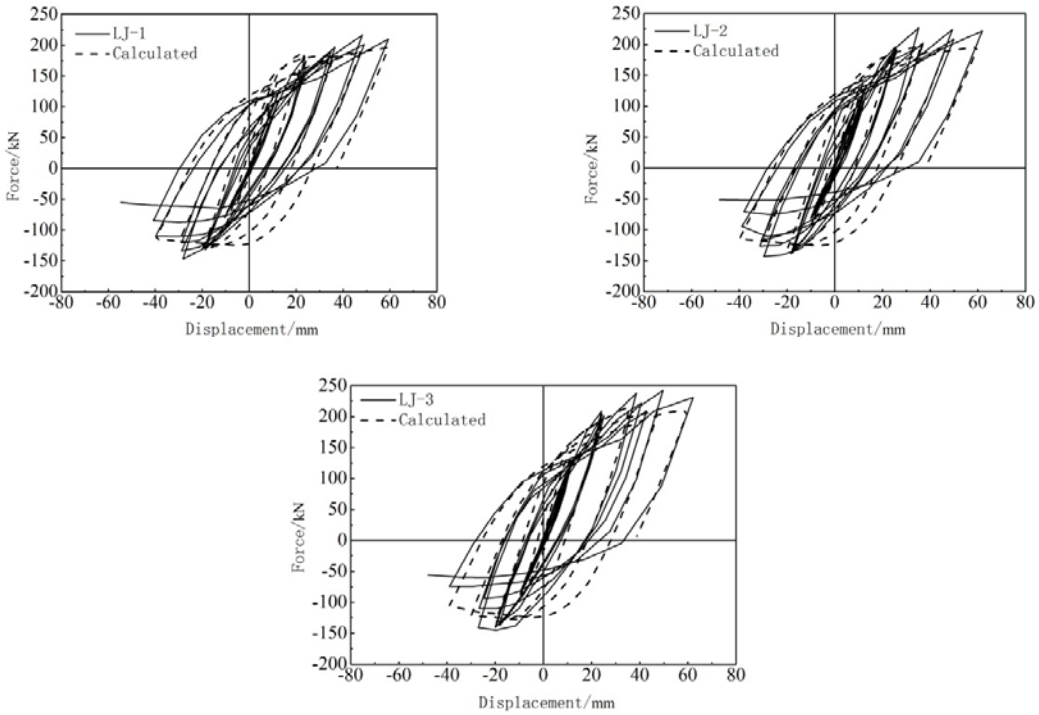

Fig. 13 Comparison of the hysteretic curves for specimens

4. The proposed restoring force model

4.1 Analysis method

The analysis method of restoring force model is presented and discussed in this section. The model of restoring force for the connections is created by fitting method with experiment and the model is simplified in order to get a proper model of the restoring force for the connections. The details as following: (a) Trilinear form with the stiffness degradation is used for the skeleton curve, because $P-\Delta$ skeleton curve and load-displacement curve under monotonic loading are very similar (Jason *et al*. 2002). (b) Every key point takes the average value of the positive and negative absolute value for every cycle. (c) The unloading rigidity among every key point is the same before it comes to the ultimate load; the unloading rigidity is degraded gradually as the increase of the displacement after it comes to the ultimate load. (d) Cyclic loading meets "peak-oriented" pattern approximately (Zona *et al*. 2008, Lou and Wang 2015).

4.2 Skeleton curve model

A series of restoring force curve models are available in literature, including the smooth-varying and piecewise-linear (PWL) varieties. The PWL model refers to the one with stiffness degradation characteristics which consist of bilinear model, trilinear model, double bilinear model and origin-oriented trilinear model. In this section, we attempt to indicate the basis of the formulation presented in the previous section by dimensionless method to present the skeleton

curve model. The skeleton curve denotes the feature points of restoring force curve. And it is a polyline with every feature points between the first loading curve and ones in hysteretic loops of the hysteretic curve. The ultimate bearing capacity and corresponding displacement are difficult to express with a general equation for three test specimens. Therefore, the tested skeleton curve is dimensionless with P/P_{max}, Δ/Δ_{max}, where P_{max} and Δ_{max} represent the ultimate bearing capacity of test specimens, and corresponding ultimate displacement. After the dimensionless of data, the model can be better expressed for hysteretic law. Then the skeleton curve is subjected to regression analysis by using trilinear model, considering the stiffness degradation after connection yield. For the trilinear model, the linear equation for every segment and slope in the skeleton curve are listed in Table 4.

Fig. 14 shows the result of trilinear skeleton curve model by using regression analysis. Lines 01 and 01' represent the loading-displacement of test specimens before they yield using regressing analysis under repeated vertical loading at the end of the beam. Their slopes represent the relative elastic stiffness of the connections. Lines 12 and 1'2' represent the regression relation between yield point and unloading stiffness point of ultimate loading under positive and negative loading respectively. The slopes represent the plastic stiffness after the connections yield. Lines 23 and 2'3' are obtained through the regressive analysis of loading versus displacement in the stage of strength degradation after the connections reaches ultimate loading. The key points 1(1') represent the positive and negative yield point, respectively showing as coordinates (P_y, Δ_y) in the skeleton curve of loading-displacement. The key points 2(2') represent the positive and negative ultimate loading point, coordinates (P_{max}, Δ_{max}).

Table 4 Regression equation of trilinear skeleton curve model

Line	Regression equation	Angle to the X-axis/(°)
01	$P/P^{+}_{max} = 1.97\,\Delta/\Delta^{+}_{max}$	63
12	$P/P^{+}_{max} = 0.47\,\Delta/\Delta^{+}_{max}+0.56$	25
23	$P/P^{+}_{max} = -0.08\,\Delta/\Delta^{+}_{max}+1.08$	-5
0'1'	$P/P^{-}_{max} = 1.48\,\Delta/\Delta^{-}_{max}$	56
1'2'	$P/P^{-}_{max} = 0.58\,\Delta/\Delta^{-}_{max}-0.46$	30
2'3'	$P/P^{-}_{max} = -0.75\,\Delta/\Delta^{-}_{max}-1.72$	-37

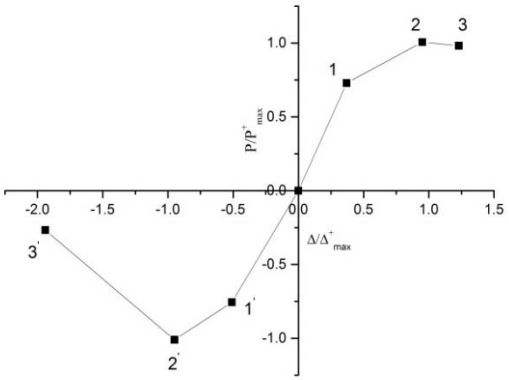

Fig. 14 Trilinear skeleton curve model

4.3 Stiffness degradation law

Comparing the trilinear skeleton curve model and loading-displacement hysteretic curve obtained from the experiment, both of the loading and unloading stiffness of the test specimens show certain degradation. Fig. 15 shows the stiffness degradation law of the connections under low cyclic and reciprocating loading, the characteristics can be simplified as follows: (a) There is no stiffness degradation when unloading. K_1 is the positive unloading stiffness. However, the stiffness will appear degradation when reverse loading after unloading to zero. (b) Unloading to zero during the inelastic range, and then reverse loading firstly, the line will direct to negative yield point, so this is the reverse loading stiffness K_2. After that, the line will direct to the maximal displacement during the following reverse loading. (c) The reverse unloading stiffness is K_3 when unloading during the test, then forward loading, the line will direct to the first positive unloading point A, this the positive loading stiffness K_4 as indicated in detail in Fig. 15.

4.4 Mathematical description of restoring force model

The real restoring force models of CFST laced columns to composite box-beam connections are shown as complicate curves and difficult in continuously and completely express with a mathematic equation, especially for the seismic analysis. So this study aims to build a practical and mathematical restoring force model for these connections, and can represent the real restoring characteristic. Fig. 16 shows the trilinear restoring force model considering a comprehensive analysis from the stiffness degradation law of the connections, hysteretic curves of test specimens to trilinear skeleton curve model mentioned above. This model can reflect the strength and stiffness law of the connections as the increasing of the displacement by using the trilinear style with degradation. And it can be used for CFST laced columns to composite box-beam connection and the structural analysis.

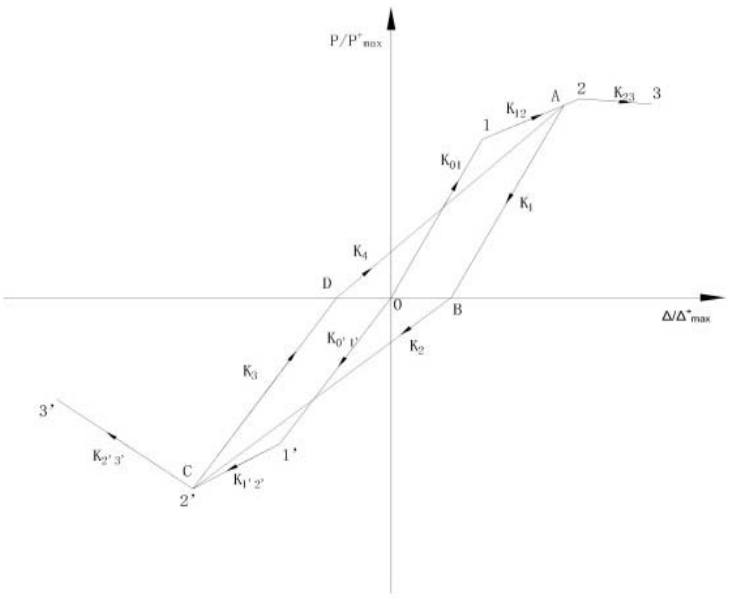

Fig. 15 Stiffness degradation law

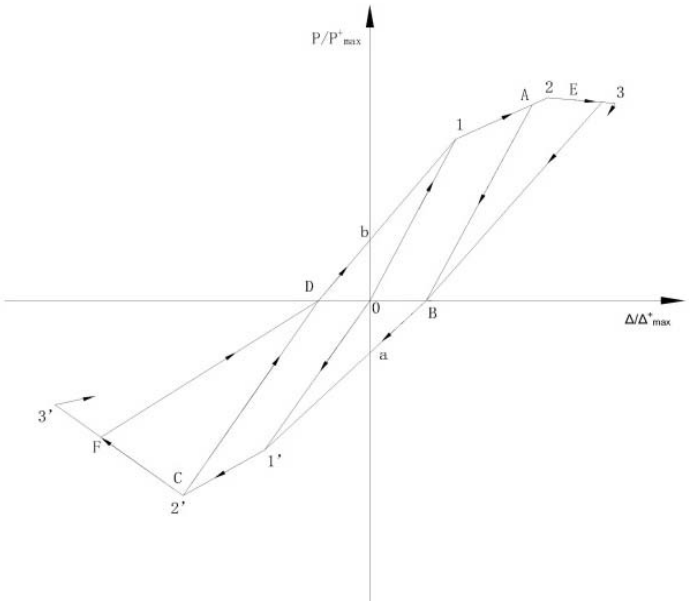

Fig. 16 Trilinear restoring force model

This section will describe the restoring model. It shows as dimensionless coordinate and fitting from feature points in the representative hysteretic loops to the shape of hysteretic curves, details shown in Fig. 16. The numbers in the turning points show the track of hysteretic curve (loading versus displacement curve). Points 1(1') represent the positive and reverse yield points respectively. From point 1 to 2 (from 1'to 2') represents the positive and negative strengthening stage respectively. Lines 23 (2'3') are corresponding to the softening stage of the connections. If unloading during the stage of lines 01 (0'1'), the unloading path is 10 (1'0). However, if unloading during the stage of lines 12 (1'2') the unloading-stiffness would show degradation as lines AB (CD). Then, reverse loading after unloading to point B, it will develop around Ba1'2'3'. Unloading when it reverse loading to lines 2'3', the unloading path is shown as FD. Then loading at this time, it will develop around Db123. This trilinear restoring force model shows a simple and distinct loading-unloading law. The stiffness is in elastic stage before the test specimens' yield. But when it goes through the yield point, the loading stiffness gradually decrease. The degradation rate increase as the cycles increase. Reverse reloading after unloading represent an obvious Bauschinger's Effect. The bearing capacity continuously decrease, but the ductility of the specimens is fairly good.

5. Validation of restoring force model and discussion

5.1 Experimental validation

A set of correlation studies between experimental data and analytical results on CFST laced columns to composite box-beam connection under cyclic loading was performed to assess the accuracy of the proposed trilinear restoring force model. The skeleton curves of specimens analyzed with regression method are compared with the experimental results in Fig. 17. The

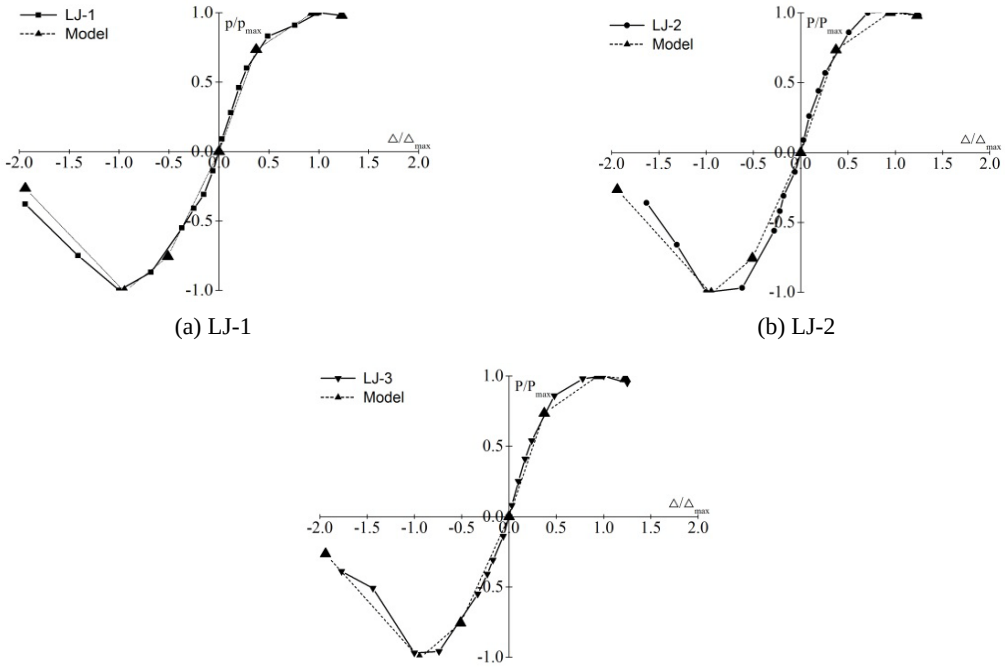

(a) LJ-1 (b) LJ-2

(c) LJ-3

Fig. 17 Comparison of the skeleton curves for specimens

trilinear restoring force model of connections can fairly reflect the relationship between loading and displacement and the rules of the real skeleton curves. The simplified trilinear lines can match the envelope curve of the skeleton curves. The comparison between theoretical and experimental result reveal: the simplified trilinear restoring force model predicted the experimental data with high accuracy. This model can be used for elastic-plastic response analysis of CFST laced column to composite box-beam connections.

5.2 Numerical simulation and analysis of restoring force model

Based on the numerical analysis in the section 3, six different connection types including single-limb bracing, cross bracing, diaphragms, no-connector, single-limb tube and cross tube for

Table 5 Types for core area of connections

Number	Types of connections for core area
LJ-1	Single-limb bracing
LJ-2	Cross bracing
LJ-3	Diaphragms
LJ-4	No connector in the core area
LJ-5	Single-limb tube
LJ-6	Cross tube

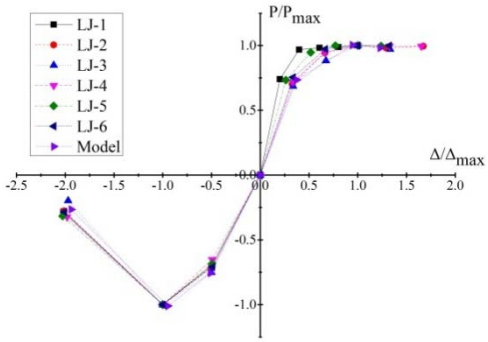

Fig. 18 Comparison of numerical analysis for connections

core area of connections (listed in Table 5) would be conducted to assess the accuracy of the proposed trilinear restoring force model. The load-displacement skeleton curves of connections by dimensionless method were extracted and compared with the trilinear restoring force model proposed in this paper in Fig. 18.

In most cases, the proposed trilinear restoring force model of connections matches the numerical simulation results well. As shown in Fig. 18, the skeleton curves obtained from the numerical simulation for all of the types of connections show the same tendency. The positive (negative) elastic stiffness, negative plastic stiffness and strength degradation of skeletons for all connection types are matched well. Although the positive plastic stiffness after the connections yields are slightly fluctuated between the connection LJ-1 and the Model, the results are still in the acceptable range. Based on the numerical analysis, the simplified trilinear restoring force model predicted the load-displacement skeleton curves with high accuracy; it can be used for elastic-plastic response analysis of CFST laced column to composite box-beam connections with different connection types in the core area.

5.3 Stiffness analysis and discussion

The ring strengthening connections are considered to be rigid joints. In order to find the optimal connection's construction for structure design, the stiffness of the six different connection types were analyzed and compared in this section. The comparison of the connections' stiffness is listed in Table 6.

The comparison shows that the positive and negative stiffness of the connections was significantly influenced by the connection's construction in the core area. The stiffness of the connections LJ-1, LJ-2, LJ-5 and LJ-6 are almost the same. However, the positive and negative stiffness of connection LJ-3 is obviously higher than others. The positive stiffness of LJ-3 with diaphragms is 25.9% higher than that of the LJ-4 with no-connector in the core area; and the negative stiffness is 23.9% higher than that also. This is because the core area of connection LJ-3 is enhanced by the diaphragms as a solid connection, and the stiffness of the solid connection is obviously stronger than the lattice connection. At the same time, the connection LJ-3 can be directly cut from the base metal according the actual size and can be welded on the construction site and these make the progress much easier, which ensures the quality of the welds. Stated thus, the diaphragm style (LJ-3) is suggested to be used in the core area of the connection in the composite structures of seismic design.

Table 6 Comparison of stiffness for connections (kN/mm)

Types	LJ-1	LJ-2	LJ-3	LJ-4	LJ-5	LJ-6
Positive stiffness	14.62	14.93	16.09	12.78	13.64	14.50
Negative stiffness	9.72	9.96	10.12	8.17	9.08	9.45

6. Conclusions

Cyclic tests of the three connections for CFST laced column to composite box-beam were carried out and characteristics in failure, hysteresis curves and skeleton curves were obtained. The new simplified trilinear restoring force model was applied to analyze the hysteretic response of these specimens. To identify the most suitable skeleton model, the regression analysis results were compared with the experimental results and numerical simulation results.

Based on the experimental study and numerical simulation, the following observations and conclusions are offered:

(1) The test specimens would fail in weak-beam failure mechanism under cyclic loading. Overall, the hysteretic loops appear full as a spindle-shape. The tiny pinch phenomenon would appear due to the uncertain pouring quality of concrete. As a result, the studied connections for CFST laced column to composite box-beam show a good seismic performance.

(2) The yield displacement of the test specimens decrease as the core area of connections is strengthening from single-limb bracing, cross bracing to diaphragms. The positive bearing capacity of the test specimens would increase gradually, while the negative bearing capacity is remain the same.

(3) Under the low cyclic loading, the stiffness would be increase gradually and the degradation of the strength and stiffness are obvious as the core area of connections is strengthening. The skeleton curves of test specimens can be divided into three stages from initial elastic, elastic-plastic, to plastic decreased stage. The positive downtrend rate of skeleton curves of the specimens is slower than the negative downtrend, it reveals that the positive plastic behavior is better than the negative one.

(4) The diaphragm style used in the core area of the connection (LJ-3) is suggested to be used to the seismic design of composite structures. In addition, the thickness of the diaphragms related to the design of compression flange for steel box beam is suggested to refer literature (GB50017 2003) to assure that neither waste construction materials nor lower the connection mechanics performance.

(5) The comparison among regression analysis, experimental results and numerical simulation results reveals: The simplified trilinear restoring force model was proposed, which predicted the experimental data and numerical simulation results accurately. And the trilinear restoring force model of connections can fairly reflect the relationship between loading and displacement and the rules of the real skeleton curves. The simplified trilinear lines can be used for elastic-plastic response analysis of CFST laced column to composite box-beam connections.

Acknowledgments

The authors would like to express their gratitude for the financial supports provided by National Natural Science Foundation of China (Grant No. 51378502, 51408449), the Special Fund of Strategic Leader in Central South University (Grant No. 2016CSU001), and China Scholarship Council. The opinions expressed in this paper are solely of the authors, however.

References

ATC-24 (1992), Applied Technology Council; Guidelines for cyclic testing of components of steel structures, Redwood City, CA, USA.

Denavit, M.D., Hajjar, J.F., Perea, T. and Leon, R.T. (2016), "Stability analysis and design of composite structures", *J. Struct. Eng.*, **142**(3), 1-12.

Esfandyary, R., Razzaghi, M.S. and Eslami, A. (2015), "A parametric investigation on the hysteretic behavior of CFT column to steel beam connections", *Struct. Eng. Mech., Int. J.*, **55**(1), 205-228.

GB/T 50081-2002 (2002), National Standard of the People's Republic of China; Standard for test method of mechanical properties on ordinary concrete, Beijing, China.

Guo, Z.H. (1998), *Reinforced Concrete Structures*, Tsinghua University Press, Beijing, China.

GB/T2975-1998 (1998), National Standard of the People's Republic of China; Steel and steel products-location and preparation of test pieces for mechanical testing, Beijing, China.

GB/T10433-2002 (2002), National Standard of the People's Republic of China; Cheese head studs for arc stud welding, Beijing, China.

GB50017-2003 (2003), National Standard of the People's Republic of China; Code for design of steel structures, Beijing, China.

Jason, B., David, T. and Nimal, P. (2001), "Monotonic behaviour of composite column to beam connections", *Eng. Struct.*, **23**(9), 1152-1161.

Jason, B., David, T. and Nimal, P. (2002), "Cyclic behaviour of concrete filled steel tubular column to steel beam connections", *Eng. Struct.*, **24**(1), 29-38.

JGJ101-96 (1996), Standard of the People's Republic of China; Specification of testing methods for earthquake resistant building, Beijing, China.

Jiang, L., Huang Z., Chen, S. and Zhou, W.B. (2014), "Tests for aseismic behavior of connection joints composed of concrete-filled steel tubular lattice columns and composite box girders", *J. Vib. Shock*, **33**(18), 156-163.

Kang, L.P., Leon, R.T. and Lu, X.L. (2015), "Shear strength analyses of internal diaphragm connections to CFT columns", *Steel Compos. Struct., Int. J.*, **18**(5), 1083-1101.

Kataoka, M.N. and El Debs, A.L.H.D. (2015), "Beam-cloumn composite connections under cyclic loading: an experimental study", *Mater. Struct.*, **48**(4), 929-946.

Li, G.Q. and Cui, D. (2008), "Experimental study on the restoring fore model of shear wall supported on the frame with steel reinforced", *J. Bldg. Struct.*, **29**(4), 73-80.

Liu, W. (2005), "Research on mechanism of concrete-filled steel tubes subjected to local compression", Ph.D. Dissertation; Fuzhou University, Fuzhou, China.

Lou, G.B. and Wang, A.J. (2015), "Studies into a high performance composite connection for high-rise buildings", *Steel Compos. Struct., Int. J.*, **19**(4), 789-809.

Men, J.J., Guo, Z.F. and Shi, Q.X. (2015), "Experimental research on seismic behavior of novel composite RCS joints", *Steel Compos. Struct., Int. J.*, **19**(1), 209-221.

Sabouri-Ghomi, S., Jahani, Y. and Bhowmick, A.K. (2016), "Partial interaction theory to analyze composite (steel-concrete) shear wall systems under pure out-of-plane loadings", *Thin-Wall. Struct.*, **104**, 211-224.

Stephen, P.S. and Yousef, M.A. (1998), "Experimental behavior of connections to concrete-filled steel tubes", *J. Constr. Steel Res.*, **45**(3), 321-352.

Wang, W. (2006), "Behaviour of steel beam to concrete-filled steel tubular columns frames", Ph.D. Dissertation; Fuzhou, Fuzhou University, Fuzhou, China.

Wu, L., Wang, X.D., Luo, S. and Wang, X. (2015), "Experimental research on seismic performance of the full bolted diaphragm-through connection to RCFST", *Adv. Struct. Eng.*, **18**(7), 959-973.

Xu, G. and Nie, J. (2011), "Experimental study of connections of concrete-filled square steel tubular columns with continuous diaphragms", *China Civil Eng. J.*, **44**(8), 25-32.

Xue, W.C. and Zhang, B. (2014), "Seismic behavior of hybrid concrete beam-column connections with composite beams and cast-in-place columns", *ACI Struct. J.*, **111**(3), 617-627.

Yousef, M.A. and Stephen, P.S. (1996), "Analytical behavior of connections to concrete-filled steel tubes", *J. Constr. Steel Res.*, **40**(2), 95-127.

Yu, Z.W. and Ding, F.X. (2003), "Unified calculation method of compressive mechanical properties of concrete", *J. Build. Struct.*, **24**(4), 41-46.

Zhang, D.X., Gao, S.B. and Gong, J.H. (2012), "Seismic behavior of steel beam to circular CFST column assemblies with external diaphragms", *J. Constr. Steel Res.*, **76**, 155-166.

Zona, A., Barbato, M. and Conte, J.P. (2008), "Nonlinear seismic response analysis of steel-concrete composite frames", *J. Struct. Eng.*, **134**(6), 986-997.

CC